DIGITAL ACCESS TO SCHOLARSHIP AT HARVARD
DASH.HARVARD.EDU

HARVARD LIBRARY
Office for Scholarly Communication

Nucleotide-dependent Domain Movement in the ATPase Domain of a Human Type IIA DNA Topoisomerase

Citation

Wei, Hua, Alexander J. Ruthenburg, Seth K. Bechis, and Gregory L. Verdine. 2005. "Nucleotide-Dependent Domain Movement in the ATPase Domain of a Human Type IIA DNA Topoisomerase." Journal of Biological Chemistry280 (44): 37041–47. https://doi.org/10.1074/jbc.M506520200.

Permanent link

http://nrs.harvard.edu/urn-3:HUL.InstRepos:41511303

Terms of Use

This article was downloaded from Harvard University's DASH repository, and is made available under the terms and conditions applicable to Other Posted Material, as set forth at http://nrs.harvard.edu/urn-3:HUL.InstRepos:dash.current.terms-of-use#LAA

Share Your Story

The Harvard community has made this article openly available.
Please share how this access benefits you. Submit a story .

Accessibility

THE JOURNAL OF BIOLOGICAL CHEMISTRY VOL. 280, NO. 44, pp. 37041–37047, November 4, 2005
© 2005 by The American Society for Biochemistry and Molecular Biology, Inc. Printed in the U.S.A.

Nucleotide-dependent Domain Movement in the ATPase Domain of a Human Type IIA DNA Topoisomerase*[S]

Received for publication, June 15, 2005, and in revised form, July 27, 2005 Published, JBC Papers in Press, August 12, 2005, DOI 10.1074/jbc.M506520200

Hua Wei[‡], Alexander J. Ruthenburg[‡1], Seth K. Bechis[‡2], and Gregory L. Verdine[‡§¶3]

From the Departments of [‡]Chemistry and Chemical Biology and [§]Molecular and Cellular Biology, Harvard University, Cambridge, Massachusetts 02138 and the [¶]Program in Cancer Chemical Biology, Dana Farber Cancer Institute, Boston, Massachusetts 02115

Type IIA DNA topoisomerases play multiple essential roles in the management of higher-order DNA structure, including modulation of topological state, chromosome segregation, and chromatin condensation. These diverse physiologic functions are all accomplished through a common molecular mechanism, wherein the protein catalyzes transient cleavage of a DNA duplex (the G-segment) to yield a double-stranded gap through which another duplex (the T-segment) is passed. The overall process is orchestrated by the opening and closing of molecular "gates" in the topoisomerase structure, which is regulated by ATP binding, hydrolysis, and release of ADP and inorganic phosphate. Here we present two crystal structures of the ATPase domain of human DNA topoisomerase IIα in different nucleotide-bound states. Comparison of these structures revealed rigid-body movement of the structural modules within the ATPase domain, suggestive of the motions of a molecular gate.

Type IIA DNA topoisomerases (Topo IIs)[4] are complex multifunctional enzymes that use the energy of ATP hydrolysis to resolve topological problems encountered in the genome during cell growth and division (reviewed in Refs. 1–3). The functions served by Topo II enzymes are essential for cell viability; hence these evolutionarily conserved enzymes have been widely exploited as targets for clinically important antibiotics and anti-tumor drugs (4). A broad range of biochemical and structural studies has provided a detailed understanding of the molecular mechanism employed by Topo II enzymes, including those of eukaryotic origin (1–3). Eukaryotic Topo II is a homodimer having two functionally distinct domains per subunit, an N-terminal ATPase domain, and a C-terminal DNA cleavage-religation domain. Structures of these individual functional domains from *Saccharomyces cerevisiae* have been solved (5–7), leading to a composite picture of Topo II as a theta-shaped dimer having three major dimer interfaces, one at the N terminus, one in the middle, and one at the C terminus. Each of the three interfaces constitutes a gate allowing capture and restricting passage of duplex DNA. In the absence of DNA and ATP, the N-terminal gate (N-gate) is open, and the middle (M-gate) and C-terminal (C-gate) gates are closed. According to the two-gate model (8), the Topo II catalytic cycle is initiated by the binding of the G-segment to the middle gate. Binding of ATP then triggers the closing of the N-gate via establishment of a dimer interface in the ATPase domain and captures the T-segment when present. Closing of the N-gate promotes the cleavage of the G segment and opening of the M-gate. The T segment then passes through the M-gate, after which the M-gate closes and the C-gate opens to allow release of the passed T-segment. Finally, the C-gate closes, and the N-gate opens to prepare for another round of strand passage (9). Following multiple rounds of T-segment passage, the G-segment is released from Topo II.

One of the central mysteries surrounding Topo II structure and function concerns the mechanisms through which nucleotide binding, hydrolysis, and release are transduced into gate opening and closure. To gain insight into this question, we solved the crystal structure of the ATPase domain of human Topo IIα (HT2ATPase, residues 29–428) bound to either AMPPNP (a non-hydrolyzable ATP analog) or ADP to 1.86 and 2.51 Å, respectively. Comparison of these two structures revealed rigid-body motions of structural modules within the ATPase domain consistent with the opening and closing of a molecular gate.

EXPERIMENTAL PROCEDURES

Plasmid Construction—The gene of HT2ATPase (residues 29–428) was amplified from YEpWOB6 (10) by PCR using two primers, 5′-CGCCGCCGCCGCCGAGCTCC*GAAAACCTGTACTTCCAGTC-TG*TTGAAAGAATCTATCAAAAGAAAAC-3′ and 5′-GCCGCCGCCGCCGCCCTCGAGTTATTATGAACACTTCTTGTTTAACTGGAC-3′. The DNA sequence corresponding to tobacco etch virus protease recognition sequence is italic. To make a plasmid that has both His and MBP tags, the MBP encoding sequence was excised from pIADL 16 vector with NcoI (New England Biolabs) and XhoI (New England Biolabs) restriction enzymes and ligated with pET 30a vector (Novagen) treated with the same restriction enzymes to produce the pSB vector. Both the PCR product and the pSB vector were then digested with SacI and XhoI and ligated to each other to produce the pSB23 vector, which encodes a fusion protein that has an N-terminal His tag followed by MBP and HT2ATPase with a tobacco etch virus protease cleavage site in between.

Expression and Purification—Rosetta(DE3)pLysS (Novagen) was transformed with pSB23. Cultures were grown in LB media at 37 °C. When A_{600} of 0.6–0.8 was achieved, isopropyl 1-thio-β-D-galactopyranoside was added to a final concentration of 1 mM. After further incubation for 10 h at 30 °C, cells were harvested by centrifugation and lysed by sonication. The fusion protein (His·MBP·HT2ATPase) was purified by a nickel-nitrilotriacetic acid column followed by a heparin column. It was then cleaved by tobacco etch virus protease (made from

* This work was supported by National Institutes of Health Grant GM044853 and by a grant from Novartis Corporation. The costs of publication of this article were defrayed in part by the payment of page charges. This article must therefore be hereby marked "*advertisement*" in accordance with 18 U.S.C. Section 1734 solely to indicate this fact.
The atomic coordinates and structure factors (codes 1ZXM, and 1ZXN) have been deposited in the Protein Data Bank, Research Collaboratory for Structural Bioinformatics, Rutgers University, New Brunswick, NJ (http://www.rcsb.org/).
[S] The on-line version of this article (available at http://www.jbc.org) contains supplemental Figs. 1 and 2.
[1] Supported by a graduate research fellowship from the National Science Foundation.
[2] Present address: Medical Scientist Training Program (M.D./Ph.D.), University of California, San Francisco, CA 94122.
[3] To whom correspondence should be addressed: Dept. of Chemistry and Chemical Biology, Harvard University, 12 Oxford St., Rm. 194, Cambridge, Massachusetts 02138. Tel.: 617-495-5323; Fax: 617-495-8755; E-mail: Gregory_verdine@ harvard.edu.
[4] The abbreviations used are: Topo, topoisomerase; N-gate, N-terminal gate; M-gate, middle gate; C-gate, C-terminal gate; AMPPNP, 5′-adenylyl-β,γ-imidodiphosphate; MBP, maltose-binding protein.

Downloaded from http://www.jbc.org/ by guest on October 8, 2019

pRK793, Scientific Reagents) with no scar into two pieces, His·MBP and HT2ATPase. His·MBP was removed when the cleavage product was run through QFF column (Amersham Biosciences). HT2ATPase was further purified by Hiload 16/60 Superdex 75 size exclusion column (Amersham Biosciences).

Crystallization and Structure Determination—HT2ATPase was concentrated to 8 mg ml^{-1} and dialyzed against 20 mM Tris, pH 7.4, 5 mM $MgCl_2$, 1 mM dithiothreitol. To get crystals of HT2ATPase bound to AMPPNP, AMPPNP (Sigma) was first added to the dialyzed protein solution to 1 mM. Crystals were grown at 4 °C using hanging drop vapor diffusion (NEXTAL crystallization tool) by mixing 2 μl of protein solution with 2 μl of well solution (4–8% polyethylene glycol 6,000, 10 mM β-mercaptoethanol). Crystals grew to a size of 150 × 150 × 1,000 μm within 2 days. The crystals belonged to the orthorhombic space group $P2_12_12_1$ (a = 70.8 Å, b = 75.3 Å, c = 164.9 Å). Crystals were transferred via several steps to a solution of 6% polyethylene glycol 6,000, 10 mM β-mercaptoethanol, 20 mM Tris, pH 7.4, 5 mM $MgCl_2$, and 30% 2-methyl-2,4-pentanediol for cryoprotection before freezing in liquid nitrogen for data collection. All data were collected at the X25 beamline of the National Synchrotron Light Source and processed using HKL2000 (11). The structure was solved by molecular replacement using the dimer of *S. cerevisiae* Topo II ATPase fragment (Protein Data Bank code 1PVG) as a search model in cross-rotation and translation function searches performed using AMoRe (12) of the CCP4 package (13).

In another experiment, ADP was added to the dialyzed protein solution to 5 mM. Crystals were grown at 20 °C using hanging drop vapor diffusion by mixing 2 μl of protein solution with 2 μl of well solution (21% polyethylene glycol 1,500, 35 mM ammonium sulfate, 100 mM Tris, pH 8.0). Crystals reached the size of 120 × 120 × 50 μm within 2 days. The crystals belonged to the monoclinic space group $P2_1$ (a = 71.0 Å, b = 90.5 Å, c = 148.3 Å, $\alpha = \gamma = 90.0°$, $\beta = 90.0°$). Crystals were transferred via several steps to a solution of 21% polyethylene glycol 1,500, 35 mM ammonium sulfate, 100 mM Tris, pH 8.0, 5 mM $MgCl_2$, 5 mM ADP, and 16% glycerol for cryoprotection. All data were collected at the Northeastern Collaborative Access Team beamline of the Advanced Photon Source and processed using HKL2000. The structure was solved by molecular replacement using the monomer of HT2ATPase·AMPPNP complex as a search model.

Refinements of both structures were carried out with Crystallography & NMR system (14) with a random subset of all data set aside for the calculation of free R factors (5% for HT2ATPase·AMPPNP complex and 7.5% for HT2ATPase·ADP complex). Manual adjustments to the models were carried out with Quanta2000 (Accelerys). The electron density in omit maps clearly showed the presence of AMPPNP or ADP in the crystal structure. After the refinement of the protein part was complete, solvent molecules were added where chemically reasonable. Data collection and model statistics for both structures are listed in TABLE ONE. Solvent-accessible surface areas were calculated using GRASP v1.3 (15).

RESULTS

Structure of the HT2ATPase·AMPPNP Complex—Diffraction data of crystals of HT2ATPase (46 kDa) grown in the presence of AMPPNP were acquired using synchrotron radiation, and the structure was solved to 1.86 Å by molecular replacement using the structure of the yeast ortholog (5) as a search model followed by iterative refinement. The final structure contains one HT2ATPase dimer per asymmetric unit; the two protomers, although not strictly identical, are sufficiently similar that the dimer possesses a distinctly C_2-symmetric overall appearance (Figs. 1 and 2*A*). The polypeptide chain folds into two discrete structural modules, with the N-terminal module (residues 29–264, *blue* and *cyan* in Fig. 1*A*) bearing the characteristic nucleotide-binding fold of the GHKL superfamily (16), so named for its founding members, DNA gyrase, Hsp90, histidine kinase, and MutL. In this case, the fold consists of an eight-stranded, mixed β-sheet backed by four α-helices. The C-terminal module (residues 265–428, *magenta* and *peach* in Fig. 1*A*) is known as the transducer for the important role it serves in communicating conformational information between the ATPase domain and the cleavage-religation domain (17–20). The core of this C-terminal module is also an α-β structure consisting of a four-stranded, mixed β-sheet with one α-helix on one face and two on the other. The electron density corresponding to the dozen residues at the C terminus of this module was strong enough to reveal an overall helical architecture but too weak to position each residue unambiguously; hence these residues (412–428 in protomer A, 406–428 in protomer B) were not included in the final model.

The heart-shaped dimer has dimensions of roughly 75 Å wide and 79 Å long when viewed from the perspective of Fig. 1*A*. The primary dimerization interface involves the nucleotide-binding modules of the two monomers and buries roughly 1,800 $Å^2$ of total solvent-accessible surface area. The N-terminal 20 residues from each monomer, comprising two short helices connected by an extended strand, interact exclusively with the nucleotide-binding module of the C_2 symmetry-related monomer. The contacts between the two transducer modules are much less extensive, burying only about 400 $Å^2$ of the total solvent-accessible surface area. Contacts are also established between the nucleotide-binding module of one monomer and the transducer module of the other monomer, and these bury ~500 $Å^2$ of the total solvent-accessible surface area. The entire dimer interface thus encompasses some 2,700 $Å^2$ of protein surface area, with half being contributed by each protomer. The HT2ATPase contains a small cavity some 17 Å wide and 14 Å high, bounded at the front and back by a 22-amino acid β-hairpin from the nucleotide-binding module of each monomer and at the sides and bottom by the transducer module. This cavity is more readily apparent in Fig. 1, *B* and *C*, in which the surface of the β-hairpin has been omitted to show the cavity more clearly. This hairpin structure is unique to eukaryotic Topo II enzymes and contains many residues that are conserved from yeast to human. The overall structure of the HT2ATPase·AMPPNP complex superimposes well with the *S. cerevisiae* Topo II ATPase·AMPPNP complex (5) (supplementary Fig. 1) with C-α root mean square deviations of 3.4 Å for the dimer and 1.8 Å for the protomer, respectively.

The nucleotide-binding mode observed here in the HT2ATPase·AMPPNP complex is quite similar to that reported for the corresponding complexes of other type II Topo ATPases (5, 21–23). Briefly, each of the monomers contains one nucleotide-binding pocket, formed mainly by residues of the nucleotide-binding module (Figs. 1*A* and 3, *A* and *B*). Three α-helices and one loop of the nucleotide-binding module form the four sides of a box-like cleft; the β-sheet element contributes the bottom, and an extended loop termed the ATP lid (16) forms the top. The adenine ring is held in place through direct hydrogen bonding to the Asn-120 side-chain carbonyl plus water-mediated contacts to the side-chain groups of Asn-120, Thr-215, and Tyr-34′ (from the other protomer). The ribose ring of the nucleotide analog appears to adopt the $C_{4'}$-*exo* sugar pucker (supplementary Fig. 2A), stabilized through hydrogen bonding of the 2′- and 3′-hydroxyls to the side chains of Ser-149 and Asn-150, respectively. Backbone amide N-H groups from six consecutive residues of the ATP-lid (residues 162–167) contact the α- and γ-phosphates of AMPPNP via their non-bridging oxyanions. The backbone N-H groups of residues 162 and 164 are also positioned

Downloaded from http://www.jbc.org/ by guest on October 8, 2019

TABLE ONE
Data collection and model statistics

	HT2ATPase·AMPPNP complex	HT2ATPase·ADP complex
Data collection		
Beamline	X-25 of the National Synchrotron Light Source	Northeastern Collaborative Access Team of the Advanced Photon Source
Space group	$P2_12_12_1$	$P2_1$
Unit cell dimensions		
a, *b*, *c* (Å)	70.8, 75.3, 164.9	71.0, 90.5, 148.3
α, β, γ (°)	90.0, 90.0, 90.0	90.0, 90.0, 90.0
Resolution (Å)[a]	50–1.86 (1.93–1.86)	50–2.51 (2.60–2.51)
Unique reflections[a]	71,651 (6,371)	61,096 (5,268)
Redundancy[a]	4.0 (2.7)	3.8 (3.8)
Completeness (%)[a]	98.5 (96.2)	99.6 (100.0)
R_{merge}[a,b]	0.078 (0.495)	0.053 (0.492)
$\langle I/\sigma \rangle$[a]	15.7 (2.5)	23.0 (2.9)
Refinement and model statistics		
Limiting resolution (Å)	1.86	2.51
R_{cryst} (%)[c]	22.0	23.5
R_{free} (%)[d]	24.3	28.1
Mean *B*-value, all atoms	37.9 (31.1)	57.9 (71.0)
(Å^2)[e,f]		
Root mean square deviations from ideality[f]		
Bond lengths (Å)	0.006	0.007
Bond angles (°)	1.22	1.28
Dihedral angles (°)	23.4	23.9
Ramachandran plot (%)[f]		
Most favored	87.6	83.1
Additionally allowed	12.1	15.9
Generously allowed	0.3	1.0
Non-water atoms	5,993	11,408
Water molecules	528	238

[a] Values in parentheses refer to the highest resolution bin.
[b] $R_{merge} = \Sigma_{hkl} |I(hkl) - \langle I(hkl) \rangle| / \Sigma_{hkl} \langle I(hkl) \rangle$.
[c] $R_{cryst} = \Sigma_{hkl} |F_o(hkl) - F_c(hkl)| / \Sigma_{hkl} |F_o(hkl)|$.
[d] R_{free} was calculated based on 5% (HT2ATPase · AMPPNP complex) or 7.5% (HT2ATPase · ADP complex) of the total data omitted during structure refinement.
[e] Values in parentheses were obtained by Wilson plot.
[f] Values provided by PROCHECK.

within hydrogen-bonding distance of the bridging β,γ-imino nitrogen of AMPPNP; these contacts are likely to be more favorable with the oxygen atom of the actual substrate ATP. Ser-148 donates a hydrogen bond to the β-phosphate, and Lys-168 and the δ^2 amide nitrogen of Asn-91 interact with the α-phosphate. An active site Mg^{2+} ion contacts all three phosphates of AMPPNP, with the δ^1 carbonyl oxygen of Asn-91 and two water molecules completing the distorted octahedral metal-ion coordination shell (Fig. 3, *A* and *B*). The floor of the nucleotide-binding pocket is lined with apolar side chains that contribute van der Waals contacts to the adenine ring and ribose moiety of the nucleotide (Fig. 3*E*). Only one contact to the nucleotide is contributed by a residue outside of the nucleotide-binding module. The highly conserved Lys-378 from the QTK-loop of the transducer domain forms a salt bridge with the γ-phosphate of AMPPNP (Fig. 3, *A* and *B*, indicated by electron density map). This salt bridge is believed to stabilize the transition state of the hydrolysis reaction because mutation of the corresponding Lys residue in DNA gyrase (K337Q) results in dramatically decreased ATPase activity while preserving the ability of the enzyme to perform DNA cleavage (24). Although mutation of this residue in *Drosphila melanogaster* Topo II (K359Q or K359E) ablates DNA-stimulated ATPase activity while retaining a basal ATP hydrolysis rate (25). The key catalytic general base (26), Glu-87, is hydrogen-bonded to one of the two water molecules coordinated to Mg^{2+}. Presumably this residue activates an attacking water molecule that is not observed in this structure.

Structure of HT2ATPase·ADP Complex—Like the HT2ATPase·AMPPNP complex, the HT2ATPase·ADP complex is a pseudosymmetric dimer (Fig. 1*D*), with two dimers per asymmetric unit. The dimers are not identical crystallographically but are similar enough that either one is representative of both. The individual protomers in the ADP complex show greater variation than in the AMPPNP complex (see Fig. 2, *B* and *A*, respectively), suggesting a less constrained overall conformation in the ADP complex. Viewed from the perspective in Fig. 1*D*, the dimer is heart-shaped and elongated relative to the AMPPNP complex (75 Å wide and 90 Å high). This elongation results primarily from the ordering of a C-terminal extension on the transducer domains that is too disordered to model in the AMPPNP complex; the extensions on each monomer contact each other at the base of the dimer to encircle completely an irregular cavity some 26 Å wide and 18 Å high at its upper end and 40 Å wide and 23 Å high at the lower end (more readily apparent in Fig. 1, *E* and *F*).

Each ligand-binding pocket (Fig. 3, *C* and *D*) contains one bound ADP molecule. The resolution of the ADP complex is not as high as that of the AMPPNP complex; thus the ADP-binding mode cannot be described in the same detail as that for AMPPNP, but the salient features of recognition are clear nonetheless. Based on proximity to side chains

Downloaded from http://www.jbc.org/ by guest on October 8, 2019

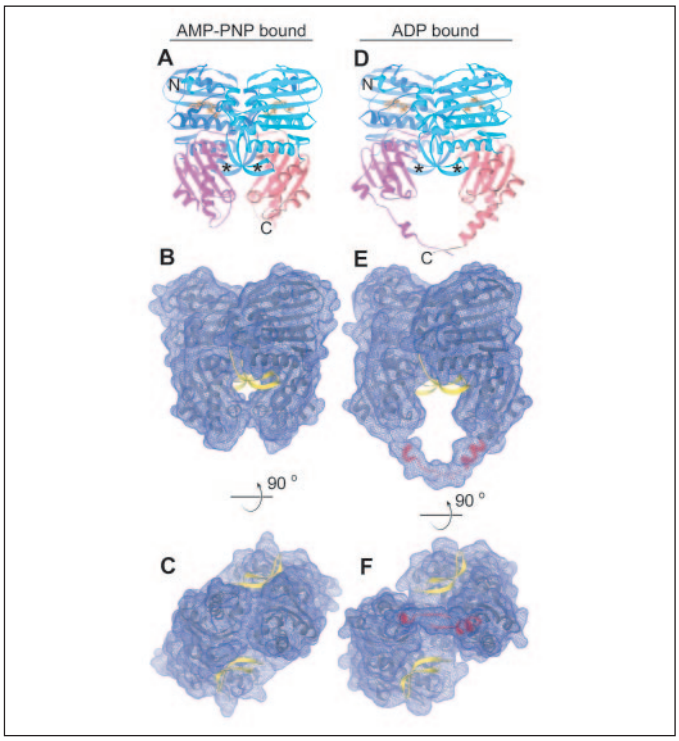

FIGURE 1. **Overall structure of the 46-kDa ATPase domain of human topoisomerase IIα (HT2ATPase) (residues 29–428) bound to AMPPNP (*A–C*) and ADP (*D–F*).** *A* and *D*, *ribbon drawings* emphasizing the modularity of the protein structure. Each of the four modules in the HT2ATPase homodimer is colored individually: *blue* and *cyan*, ATPase modules; *magenta* and *peach*, transducer modules. One protomer of HT2ATPase is *blue* and *magenta*; the other is *cyan* and *peach*. *Asterisks* denote the β-hairpin motif, unique to eukaryotic Topo II enzymes, which forms the upper end of the DNA channel. *B* and *E*, surface representation in the same orientation as *A* and *D*, with the β-hairpin shown in *yellow*. *Red* in underlying *ribbon trace* indicates C-terminal portions of the structure that become ordered in the ADP-bound state. *C* and *F*, surface drawing rotated by 90° about the *x* axis with respect to *B* and *E*, looking inward from the C terminus-proximal end of the cavity.

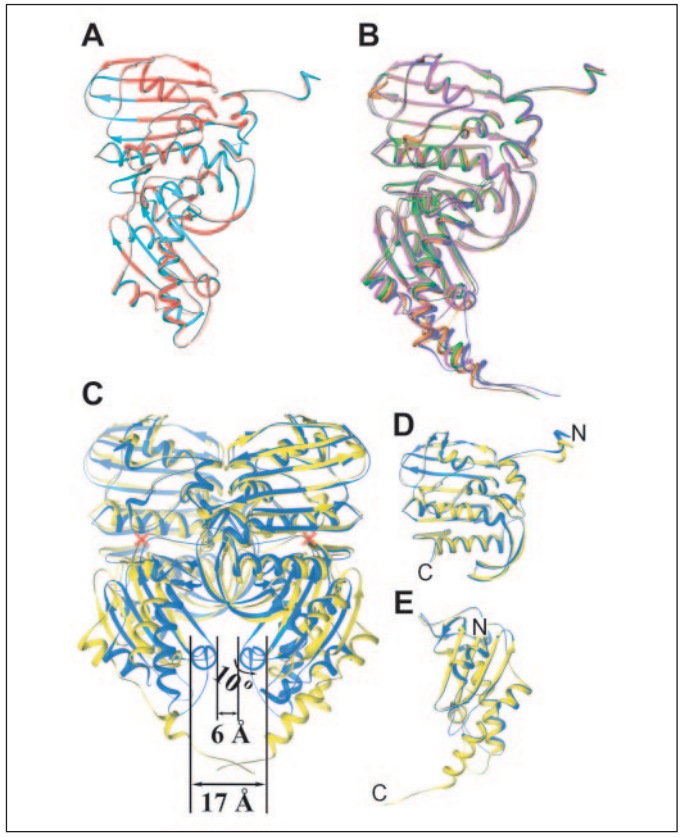

FIGURE 2. **Analysis of nucleotide-dependent domain movement in HT2ATPase.** *A*, least-squares superposition of the two protomers in the asymmetric unit of the AMPPNP structure. *B*, superposition of the four protomers in the asymmetric unit of the ADP structure. *C*, superposition of the dimers of the AMPPNP (*blue*) and ADP (*yellow*) structures. The magnitude of domain rotation and translation is indicated. *Red X* indicates the approximate pivot point for rigid-body rotation. *D* and *E*, superposition of the individual (*D*) nucleotide-binding and (*E*) transducer modules in the AMPPNP structure and ADP structure (coloring as in *C*).

on the protein, the adenine ring in the ADP complex appears to make the same set of direct and water-mediated contacts as in the AMPPNP complex; however, the bridging waters are not as evident in the former. Although the sugar pucker in the ADP complex cannot be deduced solely from the density of the furanose ring, the density for the substituents on the ring are incompatible with the $C_{4'}$-*exo* pucker seen in the AMPPNP complex and are most consistent with a $C_{3'}$-*exo* pucker (supplementary Fig. 2B). The contacts to both the α- and β-phosphate are the same in the ADP complex as in the AMPPNP complex, with the exception that the ADP complex has an additional hydrogen bond between the β-phosphate and the Asn-150 side chain; this is made possible by the disengagement of Asn-150 from the 2′-OH upon flipping from the 2′-*exo* to 2′-*endo* pucker. The details of Mg^{2+} ion coordination are also nearly identical in the two complexes, except that a water molecule fills the coordination site vacated by the γ-phosphate oxygen. Although the ATP-lid has lost three hydrogen-bonding contacts to the γ-phosphate, the lid remains in place because of the preservation of multiple contacts with the α- and β-phosphates.

Nucleotide-dependent Structural Reorganization—Superposition of the structures of the two complexes reveals significant changes in overall conformation (Fig. 2*C*). Although the nucleotide-binding modules superimpose very well, the transducer domain of each monomer of the ADP complex swings out by about 10°, increasing the width of the channel at the most narrow point from 6 to 17 Å. To assess whether this conformational change results from rigid-body movement of the nucleotide-binding modules with respect to the transducer modules, individual modules of the AMPPNP complex were superposed individually with their counterparts in the ADP complex (Fig. 2, *D* and *E*). This superimposition shows clearly that the individual modules possess nearly identical overall structures; the average root mean square deviations of C-α atoms between the nucleotide-binding domains is 0.82 Å, and that between the transducer domains is 1.84 Å.

As mentioned above, the nucleotide-dependent domain movement is also associated with an apparent difference in domain mobility. Whereas the two monomers in the asymmetric unit of the AMPPNP complex overlay with C-α root mean square deviations of 0.72 Å, the four monomers of the ADP complex overlay with root mean square deviations of 1.22 Å (see Fig. 2, *A* and *B*, respectively).

To gain a better sense of the subtle structural changes in the nucleotide-binding site that give rise to rigid-body domain motions in the transducer module, we superimposed the nucleotide-binding sites of both complexes (Fig. 4). The architectures of the active sites are very similar. The nucleotide, the Mg^{2+} ion, and many key residues of the active site (Glu-87, Asn-91, Asn-120, Ser-148, Lys-168) are in essentially the same position in both structures. The difference in sugar pucker is associated with some local adjustments in contacts to the sugar and β-phosphate but has remarkably little effect on the relative positioning of the key recognition elements in the nucleotide, namely its adenine and phosphate anhydride moieties (Fig. 4*B*). The γ-phosphate of AMPPNP is replaced by what appears to be a water molecule in the HT2ATPase·ADP complex. The only nucleotide contact residue that

Downloaded from http://www.jbc.org/ by guest on October 8, 2019

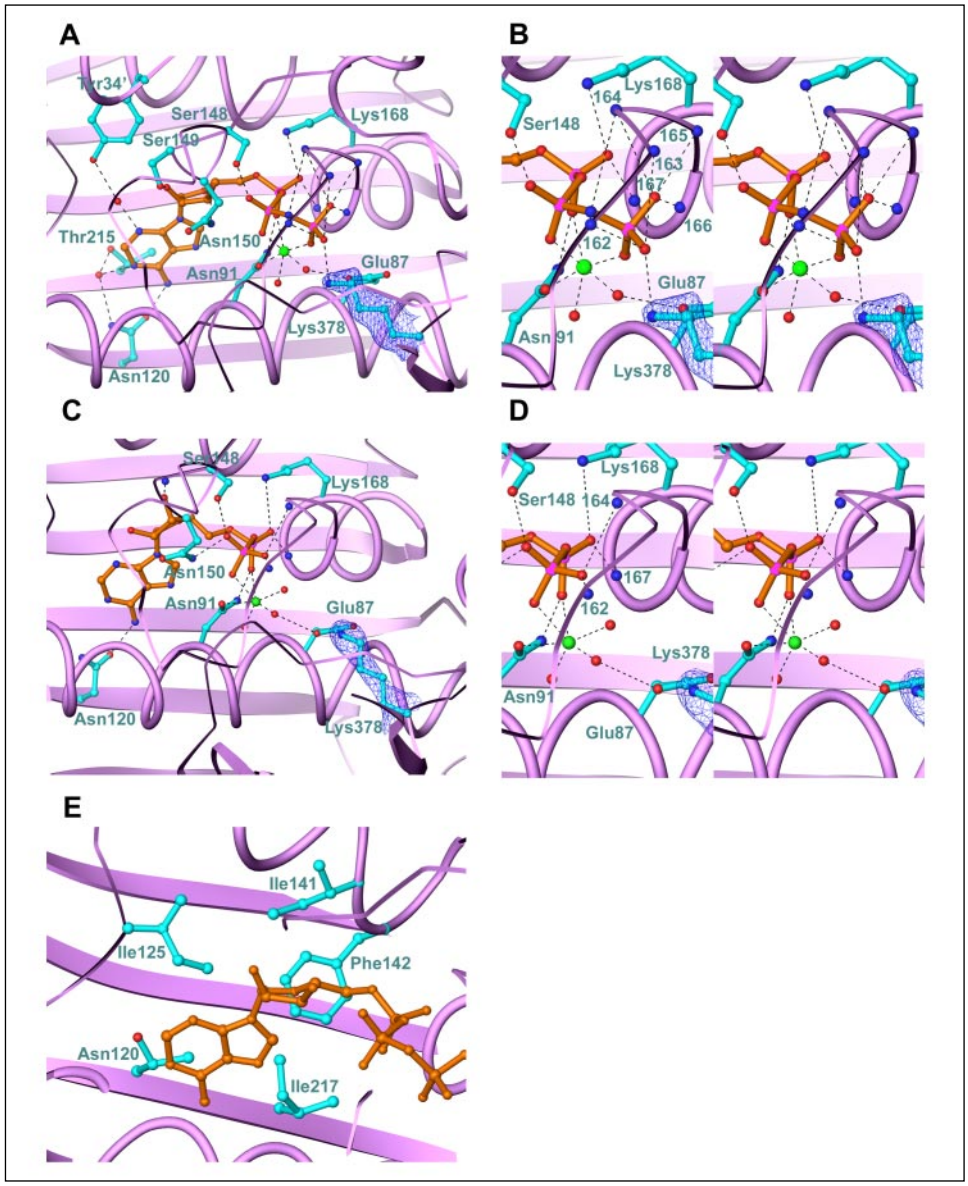

FIGURE 3. **Close-up views of the nucleotide-binding site.** In *A–E*, the protein backbone is in *magenta*, key side chains are in *cyan*, and the nucleotide is in *gold*; heteroatoms of key elements of the protein side chains and backbone, the nucleotide, and ordered/coordinated waters are colored with oxygen atoms in *red* and nitrogen atoms in *blue*, phosphorus atoms in *pink*, and the Mg^{2+} ion, *green sphere*. *A*, close-up of the AMPPNP active site and *B*, stereoview showing the interactions with the P-PNP segment of AMPPNP; in *A* and *B*, electron density for the side chain of Lys-378 is shown explicitly ($2F_o - F_c$, contour level 1.2 σ). *C*, close-up view of the ADP structure, depicted as in *A*. *D*, stereoview of the ADP structure, depicted as in *B*. In *C* and *D*, electron density for the side chain of Lys-378 is shown explicitly ($2F_o - F_c$, contour level 1.0 σ). *E*, residues of the protein that contribute non-polar interactions with the nucleotide cofactor, primarily involving the adenine ring.

undergoes a major change in contact status and position is precisely the single residue from the transducer module that makes a nucleotide contact, Lys-378. This residue, which is absolutely conserved in all type II topoisomerases, forms a salt bridge to the γ-phosphate in the AMPPNP structure. The rigid-body movement of the transducer module relative to the nucleotide-binding module in the ADP structure retracts Lys-378 away from the nucleotide. In one of the two dimers in the asymmetric unit of the ADP complex, both Lys-378 side chains are disordered; in the other dimer, each side chain is ordered and pointing toward the nucleotide but is retracted by 2.6 Å relative to its position in the AMPPNP complex (Fig. 4). In the AMPPNP complex, the distance between the Lys-378 ϵ-amino nitrogen and the nearest γ-phosphate oxygen atom is 2.6 Å, consistent with a hydrogen bond between the two. If the transducer module were to adopt the conformation observed in the ADP complex but instead bound an ATP nucleotide the distance between the Lys-378 ϵ-amino nitrogen and the nearest γ-phosphate oxygen atom would be 4.2 Å (Fig. 4*B*), as determined by modeling on the basis of the present structures. Because this region of the structure is exposed to solvent, a separation of 4.2 Å between the Lys-378 ϵ-N and the ATP γ-phosphate in the retracted state would be unlikely to produce a significant hydrogen-bonding interaction. We thus propose that the Lys-378 ϵ-N acts as both a sensor and a relay for the nucleotide-bound status of the protein, drawing the transducer domains inward upon interaction with the γ-phosphate on ATP and allowing outward movement in the absence of such a stabilizing electrostatic interaction.

DISCUSSION

Topo II performs a complex multistep reaction sequence on the genome involving introduction of a double strand break in one segment (G-segment) of the bound DNA substrate, passage of another duplex segment (T-segment) through the break, and religation of the break to restore the continuity of the DNA backbone (Fig. 5). The enzyme is believed to accomplish this difficult operation by opening and closing three different gates consisting of dimer interfaces at distinct points in the protein structure (9). The management of these gates, and hence the precise orchestration of strand scission/religation and passage, is controlled by the hydrolysis of ATP to ADP and inorganic phosphate. By analogy to other nucleotide-dependent switching proteins, it has been suspected for some time that the nucleotide hydrolysis cycle drives conformational changes in the ATPase domain of Topo II, but the nature of

Downloaded from http://www.jbc.org/ by guest on October 8, 2019

these conformational changes has remained unelucidated, as has the mechanism by which these changes enable regulated strand passage. Here we have determined the structure of the human Topo IIα ATPase domain with two different bound nucleotides, the ATP analog AMP-PNP and the hydrolysis product ADP. The former structure is very similar to that determined previously for the AMPPNP-bound state of yeast Topo II ATPase (5), whereas the latter structure represents the first observation of the product state of the ATPase domain of the type IIA DNA topoisomerases. Comparison of these structures reveals a nucleotide-dependent rigid-body movement of the transducer module relative to the nucleotide-binding module; in the ADP state, the cavity is relatively open and conformationally mobile, and in the AMPPNP (ATP-like) state the cavity is relatively closed and conformationally fixed. Similar module motion has been found in the monomeric form of *Sulfolobus shibatae* Topo VI (a type IIB Topo) B subunit (22, 27) and *Thermus thermophilus* GyrB in complex with novobiocin (28). The structures thus suggest that hydrolysis of ATP to ADP or phosphate release is associated with the opening of the cavity between the N-gate and M-gate in Topo II. Without the structure of the full-length protein dimer with DNA in a variety of ATP hydrolysis states, it is impossible to conclude how ATP hydrolysis is conformationally transduced to the cleavage-religation core. However, the differences between the two structures presented here are clearly suggestive of and are readily incorporated into the current two-gate model.

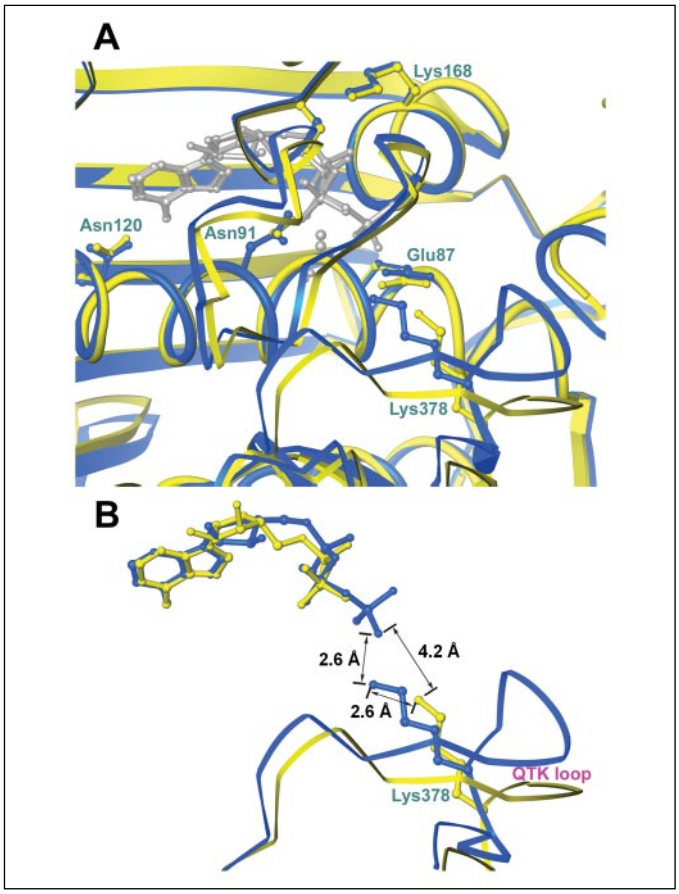

FIGURE 4. **Nucleotide-dependent changes in the active site of HT2ATPase.** *A*, superposition of the nucleotide-binding sites of the AMPPNP structure (*blue*) and ADP structure (*yellow*). In both structures, the nucleotide is in *gray*. *B*, superposition showing only the nucleotide and region around Lys-378. Distance measurements are made using the ϵ-amino of Lys-378 and the nearest γ-phosphate oxygen.

How does the cavity opening observed in the present structures fit into the larger picture of Topo II function? A model for the Topo II catalytic cycle that incorporates our findings together with those of previous studies (1–3, 5, 7–9, 18, 20, 25, 29–43) is illustrated in Fig. 5. The G-segment is known to load onto TopoII before the T-segment (41). Dimerization of the ATPase domain is nucleotide-dependent (35–37, 44). Loading of ATP onto the ATPase domain triggers dimerization and temporal capture of the T-segment in the uppermost chamber of the structure (45, 46). Interestingly, the cavity in the AMPPNP-bound HT2ATPase (17 Å wide) is not large enough to accommodate a DNA duplex (~20 Å wide); thus the cavity must expand beyond what is observed in our AMPPNP structure to accommodate the DNA, as first noted by Wigley *et al.* for GyrB (23). The present structures indicate that expansion is likely to occur by rigid-body displacement of the transducer module. In the ATP-bound state, rigid-body displacement of the transducer module would result in retraction of the Lys-378 ϵ-amino group from the γ-phosphate. There is little doubt that such movement of Lys-378, a residue that is essential for ATPase activity, would affect catalysis, but it is impossible at this stage to conclude whether the movement would decelerate ATP hydrolysis or accelerate it. Whatever the case, the structures establish the notion that transducer movement can influence ATP hydrolysis and that ATP hydrolysis in turn allows relaxation of the transducer domains to an open conformation.

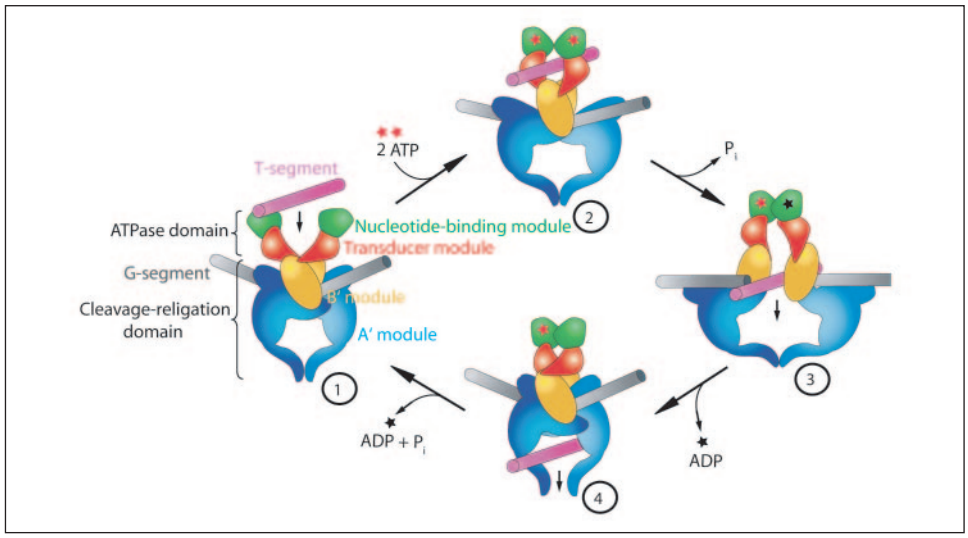

FIGURE 5. **Model for nucleotide-dependent DNA translocation by Topo II, incorporating the present findings.** The ATPase domain is depicted schematically in the context of the full protein dimer (nucleotide binding module in *green*, transducer module in *red*). The remainder of the protein, known as the cleavage-religation core, comprises the module directly C-terminal to the ATPase (B′ cleavage-reunion module, *yellow*) and a domain that bears homology to gyrase A (A′ cleavage-reunion module, *blue*). *Step 1*, G-segment DNA (*gray*) binds to the topoisomerase II dimer at the second gate of the cleavage-reunion core. *Step 2*, an incoming T-segment of DNA (*pink*) is captured in the upper cavity between the upper and middle gates by ATP (*red star*) binding-promoted dimerization. *Step 3*, hydrolysis and release of one of the two bound ATP molecules to ADP (*black star*) and P_i lead to an asymmetric retraction of the catalytic Lys-378, opening of the enzyme-bridged middle gate of the protein·DNA complex, and movement of the T-segment from the upper cavity formed in the ATPase domain into the lower cavity formed by the cleavage-reunion core. *Step 4*, hydrolysis of the remaining ATP and opening of the bottom gate allow for T-segment egress from the complex and resetting the system.

Downloaded from http://www.jbc.org/ by guest on October 8, 2019

The present structures suggest the need for transducer movement to accommodate a DNA duplex, but they provide no insight into whether one or both transducers move. The fact that ATP hydrolysis occurs sequentially (30–33) raises the intriguing possibility that only one of the two transducer modules swings outward, and it is this structural asymmetry that gives rise to catalytic asymmetry in the ATPase activity. Whatever the origins of sequential hydrolysis, the present structures predict that the transducer module of the ADP-bound protomer (and for similar reasons, the nucleotide-free protomer) is the one that swings out to expand the cavity. Even though the ADP/ADP-bound state captured here structurally is not believed to represent an actual intermediate in the overall reaction scheme, the nucleotide-dependent movement of the transducer module is likely to occur similarly in the ADP-bound protomer of the ATP/ADP state. We assert this because the nucleotide-bound status (ATP *versus* ADP) has a negligible effect on the structure of the nucleotide binding/dimerization module, and its effects are almost entirely localized to a specific pivot point in the transducer module. There is good reason therefore to expect that the ability of Lys-378 ϵ-N to act as both a sensor and a relay for nucleotide status operates independently in the two protomers.

After the expansion of the upper cavity mediated by the motion of the transducer domain, inorganic phosphate is released, the central gate opens, and the T-segment is passed into the lower chamber. ADP then dissociates from the enzyme, but the upper gate remains closed because a single bound ATP is sufficient to promote dimerization of the enzyme (29, 43). The lower chamber opens and releases the T-segment from the complex; the remaining ATP undergoes hydrolysis, and the protein·DNA complex is poised to receive another T-segment.

Acknowledgments—We thank Prof. James C. Wang for kindly providing us the human Topo IIα-containing plasmid YEpWOB6. The AMPPNP complex data for this study were measured at beamline X25 of the National Synchrotron Light Source (supported principally by the Offices of Biological and Environmental Research and of Basic Energy Sciences of the U. S. Department of Energy and by the National Center for Research Resources of the National Institutes of Health). The ADP complex work is based upon research conducted at the Northeastern Collaborative Access Team beamlines of the Advanced Photon Source, supported by award RR-15301 from the National Center for Research Resources at the National Institutes of Health. Use of the Advanced Photon Source is supported by the U. S. Department of Energy, Office of Basic Energy Sciences under Contract W-31-109-ENG-38. We thank M. Becker and the staff of the X25 beamline at the National Synchrotron Light Source and N. Sukumar and the staff of Northeastern Collaborative Access Team of the Advanced Photon Source for assistance with data collection. We also thank D. M. Graybosch and A. Banerjee for critically reading the manuscript.

REFERENCES

1. Wang, J. C. (1998) *Q. Rev. Biophys.* **31,** 107–144
2. Champoux, J. J. (2001) *Annu. Rev. Biochem.* **70,** 369–413
3. Corbett, K. D., and Berger, J. M. (2004) *Annu. Rev. Biophys. Biomol. Struct.* **33,** 95–118
4. Topcu, Z. (2001) *J. Clin. Pharm. Ther.* **26,** 405–416
5. Classen, S., Olland, S., and Berger, J. M. (2003) *Proc. Natl. Acad. Sci. U. S. A.* **100,** 10629–10634
6. Berger, J. M., Gamblin, S. J., Harrison, S. C., and Wang, J. C. (1996) *Nature* **379,** 225–232
7. Fass, D., Bogden, C. E., and Berger, J. M. (1999) *Nat. Struct. Biol.* **6,** 322–326
8. Roca, J., Berger, J. M., Harrison, S. C., and Wang, J. C. (1996) *Proc. Natl. Acad. Sci. U. S. A.* **93,** 4057–4062
9. Roca, J. (2004) *J. Biol. Chem.* **279,** 25783–25788
10. Wasserman, R. A., Austin, C. A., Fisher, L. M., and Wang, J. C. (1993) *Cancer Res.* **53,** 3591–3596
11. Otwinowski, Z., and Minor, W. (1997) *Methods Enzmol.* **276,** 307–326
12. Navaza, J. (1994) *Acta Crystallogr. Sect. A* **50,** 157–163
13. (1994) *Acta Crystallogr. Sect. D* **50,** 760–763
14. Brünger, A. T. (1998) *Acta Crystallogr. Sect. D* **54,** 905–921
15. Nicholls, A., Sharp, K., and Honig, B. (1991) *Proteins* **11,** 281–296
16. Dutta, R., and Inouye, M. (2000) *Trends Biochem. Sci.* **25,** 24–28
17. Walker, J. V., Nitiss, K. C., Jensen, L. H., Mayne, C., Hu, T., Jensen, P. B., Sehested, M., Hsieh, T., and Nitiss, J. L. (2004) *J. Biol. Chem.* **279,** 25947–25954
18. Oestergaard, V. H., Bjergbaek, L., Skouboe, C., Giangiacomo, L., Knudsen, B. R., and Andersen, A. H. (2004) *J. Biol. Chem.* **279,** 1684–1691
19. Oestergaard, V. H., Giangiacomo, L., Bjergbaek, L., Knudsen, B. R., and Andersen, A. H. (2004) *J. Biol. Chem.* **279,** 28093–28099
20. Bjergbaek, L., Kingma, P., Nielsen, I. S., Wang, Y., Westergaard, O., Osheroff, N., and Andersen, A. H. (2000) *J. Biol. Chem.* **275,** 13041–13048
21. Bellon, S., Parsons, J. D., Wei, Y., Hayakawa, K., Swenson, L. L., Charifson, P. S., Lippke, J. A., Aldape, R., and Gross, C. H. (2004) *Antimicrob. Agents Chemother.* **48,** 1856–1864
22. Corbett, K. D., and Berger, J. M. (2003) *EMBO J.* **22,** 151–163
23. Wigley, D. B., Davies, G. J., Dodson, E. J., Maxwell, A., and Dodson, G. (1991) *Nature* **351,** 624–629
24. Smith, C. V., and Maxwell, A. (1998) *Biochemistry* **37,** 9658–9667
25. Hu, T., Chang, S., and Hsieh, T. (1998) *J. Biol. Chem.* **273,** 9586–9592
26. Jackson, A. P., and Maxwell, A. (1993) *Proc. Natl. Acad. Sci. U. S. A.* **90,** 11232–11236
27. Corbett, K. D., and Berger, J. M. (2005) *Structure (Camb.)* **13,** 873–882
28. Lamour, V., Hoermann, L., Jeltsch, J. M., Oudet, P., and Moras, D. (2002) *Acta Crystallogr. Sect. D Biol. Crystallogr.* **58,** 1376–1378
29. Skouboe, C., Bjergbaek, L., Oestergaard, V. H., Larsen, M. K., Knudsen, B. R., and Andersen, A. H. (2003) *J. Biol. Chem.* **278,** 5768–5774
30. Baird, C. L., Gordon, M. S., Andrenyak, D. M., Marecek, J. F., and Lindsley, J. E. (2001) *J. Biol. Chem.* **276,** 27893–27898
31. Baird, C. L., Harkins, T. T., Morris, S. K., and Lindsley, J. E. (1999) *Proc. Natl. Acad. Sci. U. S. A.* **96,** 13685–13690
32. Harkins, T. T., and Lindsley, J. E. (1998) *Biochemistry* **37,** 7292–7298
33. Harkins, T. T., Lewis, T. J., and Lindsley, J. E. (1998) *Biochemistry* **37,** 7299–7312
34. Morais Cabral, J. H., Jackson, A. P., Smith, C. V., Shikotra, N., Maxwell, A., and Liddington, R. C. (1997) *Nature* **388,** 903–906
35. Hammonds, T. R., and Maxwell, A. (1997) *J. Biol. Chem.* **272,** 32696–32703
36. Gardiner, L. P., Roper, D. I., Hammonds, T. R., and Maxwell, A. (1998) *Biochemistry* **37,** 16997–17004
37. Campbell, S., and Maxwell, A. (2002) *J. Mol. Biol.* **320,** 171–188
38. Maxwell, A. (1996) *Nat. Struct. Biol.* **3,** 109–112
39. Lindsley, J. E. (1996) *Proc. Natl. Acad. Sci. U. S. A.* **93,** 2975–2980
40. Lindsley, J. E., and Wang, J. C. (1993) *J. Biol. Chem.* **268,** 8096–8104
41. Roca, J., and Wang, J. C. (1992) *Cell* **71,** 833–840
42. Lindsley, J. E., and Wang, J. C. (1991) *Proc. Natl. Acad. Sci. U. S. A.* **88,** 10485–10489
43. Lindsley, J. E., and Wang, J. C. (1993) *Nature* **361,** 749–750
44. Hu, T., Sage, H., and Hsieh, T. S. (2002) *J. Biol. Chem.* **277,** 5944–5951
45. Corbett, A. H., Zechiedrich, E. L., and Osheroff, N. (1992) *J. Biol. Chem.* **267,** 683–686
46. Tingey, A. P., and Maxwell, A. (1996) *Nucleic Acids Res.* **24,** 4868–4873

Downloaded from http://www.jbc.org/ by guest on October 8, 2019

Nucleotide-dependent Domain Movement in the ATPase Domain of a Human Type IIA DNA Topoisomerase

Hua Wei, Alexander J. Ruthenburg, Seth K. Bechis and Gregory L. Verdine

J. Biol. Chem. 2005, 280:37041-37047.
doi: 10.1074/jbc.M506520200 originally published online August 12, 2005

Access the most updated version of this article at doi: 10.1074/jbc.M506520200

Alerts:
- When this article is cited
- When a correction for this article is posted

Click here to choose from all of JBC's e-mail alerts

Supplemental material:
http://www.jbc.org/content/suppl/2005/08/15/M506520200.DC1

This article cites 46 references, 21 of which can be accessed free at
http://www.jbc.org/content/280/44/37041.full.html#ref-list-1

Downloaded from http://www.jbc.org/ by guest on October 8, 2019